

Morphology tuned ZnS nanostructures for hydrogen gas sensing

M. Hafeez · U. Manzoor · A. S. Bhatti

Received: 12 November 2010 / Accepted: 25 March 2011 / Published online: 9 April 2011
© Springer Science+Business Media, LLC 2011

Abstract In this paper we present the effect of dimensionality of ZnS nanostructures on hydrogen gas sensing characteristics. Vapor Liquid Solid growth mode was employed to synthesize ZnS nanostructures with different dimensions by controlling the growth parameters, *i.e.*, variation in the substrate temperature and the carrier gas flow rate. The growth was explained by using the chemical tension model and the saturation conditions were determined for each growth. X-ray diffraction and scanning electron microscopy were used to determine the phase, shape, size and density of the nanostructures. Optical properties of nanostructures also confirmed the presence of different phases of ZnS. A variety of these nanostructures were tested for hydrogen gas sensing. The rapid response time was obtained for nanowires in few hundred millisecond's range with a sensitivity of 8, which was due to its high aspect ratio as compared to the other nanostructures.

1 Introduction

The rapid developments in the synthesis and assembly of nanoscale materials will not replace immense efforts being pursued in nanofabrication. In fact, much of our understanding of the nanoscale materials is improved by the synergistic efforts of both bottom-up and top-down methods of building nanostructures. Quantum dots and quantum wires can now be produced in large quantities, and their band structures can precisely be engineered for the desired

properties. The high surface to volume ratio and high surface energies of nanostructures can be used for sensing, *e.g.*, gas sensing, chemical sensing, etc. Hydrogen (H_2) is probably to displace hydrocarbons and to become a common fuel in the future. It is an invisible, odorless, and highly inflammable gas, which makes the detection of hydrogen leakage in the environment very vital. There is a strong need to develop novel hydrogen sensors. Different materials are being used as hydrogen gas sensors with different morphology like ZnS nanobelts, ZnO nanorods, SnO_2 nanowires etc. [1–3].

ZnS is a promising wide band gap semiconductor with zinc blend structure at room temperature. It undergoes a transformation from zinc blend to Wurtzite (hexagonal) crystal structure at about 1,020 °C [4, 5]. The zinc blend and Wurtzite phases have energy band gaps of 3.6 and 3.91 eV, respectively [6]. ZnS is a good photoluminescent material and has a wide range of applications in lasers, and flat-panel displays [7–10]. It also exhibits a strong piezoelectric characteristic, which has potential applications in sensors, actuators, etc. [11].

ZnS has excellent optical properties at the nanoscale and the doped ZnS nanostructures have been used in photonic devices due to emission in the visible range [12, 13]. ZnS nanobelts have shown high-speed sensing response to sense UV light and the photoconductivity response of an individual ZnS nanobelt UV sensor is found completely reversible and periodic [14]. ZnS nanobelts based hydrogen gas sensor has also shown faster response than ZnO nanobelts [1]. ZnS has three fast growing directions, [0001], [01 $\bar{1}$ 0] and [21 $\bar{1}$ 0] which determine the length, width and the height of the nanostructures, respectively. Among these, [0001] is the fastest growing direction along c-axis with low activation temperature [5]. Thus, the final morphology of ZnS nanostructures depends on the growth

M. Hafeez · U. Manzoor · A. S. Bhatti (✉)
Department of Physics, Center for Micro & Nano Devices,
COMSATS Institute of Information Technology, Park Road
Campus, Islamabad 44000, Pakistan
e-mail: asbhatti@comsats.edu.pk

temperature due to variation in the activation energies of the different growth directions [15], which could lead to rapid or slow growth.

Vapor Liquid Solid (VLS) mechanism is the most simple technique to synthesize highly crystalline and ultra long one dimensional (1-D) nanostructures in relatively large quantities [16]. The growth kinetics of VLS suggests that the growth is highly dependent on the substrate temperature, carrier gas flow rates and the radius of the catalyst droplet. The driving force for the growth of nanowires is the supersaturation in the surrounding of the catalyst droplet, which is high outside the droplet. The best catalyst has an ideal rough surface where sticking coefficient is close to 1 [17]. Different kinds of metals have been used as catalysts but Au is the most widely used due to its interesting chemical properties, high accommodation coefficient, surface tension and wetting ability [18]. Sn and some organic materials have also been used for the growth of well aligned 1-D nanostructures [19, 20].

The chemical tension model has successfully been used to explain the growth of nanowires [21], which is based on the concept of minimization of the Gibbs free energy. The chemical tension σ^c is given by

$$\sigma^c = -l_o \frac{K_B T}{\Omega} \ln \eta + \frac{l_o \sigma_{vs}}{r} \tag{1}$$

here $\eta = \frac{p^{ZnS}}{p_{eq}^{ZnS}}$ represents the supersaturation, p^{ZnS} is the vapor pressure of ZnS and p_{eq}^{ZnS} is the equilibrium vapor pressure of ZnS, l_o is the thickness, σ_{vs} is the surface tension of the vapor–solid interface, Ω is the volume of the unit cell, r is the radius of the droplet and T is the substrate temperature.

The nanowires will grow if $\sigma^c < 0$, and if $\sigma^c > 0$, nanohillock growth will be more favorable. Equation 1 shows the nanowire growth dependence on temperature, supersaturation and the diameter of the droplet which leads to the growth rate determination [22].

$$V_n^{\frac{1}{2}} = \frac{\Delta\mu_o}{K_B T} b^{\frac{1}{n}} - \frac{4\Omega\sigma_{vs}}{K_B T} b^{\frac{1}{n}} \frac{1}{d} \tag{2}$$

where $\Delta\mu$ is the effective difference between the chemical potential of ZnS in the vapor phase and in whisker, b and n are the fitting parameters.

In this paper, ZnS nanostructures with different morphologies are synthesized by varying the growth conditions, i.e., substrate temperature and the carrier gas flow rate. X-ray diffraction and scanning electron microscopy is employed to determine the structure of the grown nanostructures. The growth conditions are used to determine the supersaturation conditions for the growth of different morphologies. The optical properties of the as-grown nanostructures are presented and analyzed with respect to the growth conditions. Finally the response of nanostructures to

hydrogen gas was determined and related to the morphology of nanostructures.

2 Experiment

Si (100) substrates having a very thin native oxide layer (2–3 nm) were used for the growth of nanostructures. 5 Å Au was deposited as catalyst at 10^{-7} Torr at 300 K. The Au coated substrates were then placed in a horizontal tube furnace along with 4 N pure ZnS powder (0.3 g) in an alumina boat, which was placed at the center of the tube. For each growth, the measured substrate temperatures were 850 ± 2 , 675 ± 2 and 460 ± 2 °C. ZnS powder was then heated at 1,020 °C in the presence of flowing carrier gas ($N_2 + 5\%H_2$) for 3 h. During the experiment, flow rate was controlled from 2 to 60 Sccm. After the growth, the left over quantities of raw material were found to be 0.286, 0.213 and 0 gm for 2, 20 and 60 Sccm flow rates, respectively.

Figure 1 shows the plot of the calculated growth rate using the Eq. (2), where $\sigma_{vs} = 0.57 \text{ Jm}^{-2}$, and $\Omega = 39.5 \times 10^{-30} \text{ m}^{-3}$ [23]. Horizontal lines show the length of a wire of diameter 120 nm at different values of supersaturation. It can be seen that higher the supersaturation, the greater is the length of the wire. In the present case the supersaturation condition is expected to be between 15 and 20 as ZnS nanowires grown were 50 μm or longer on average. For dots, the supersaturation condition determined from the size of the dots was found less than 5.

The synthesized nanostructures were characterized by using the Hitachi S4800 scanning electron microscope (SEM) and PANanalytical X-Pert XRD for the imaging and

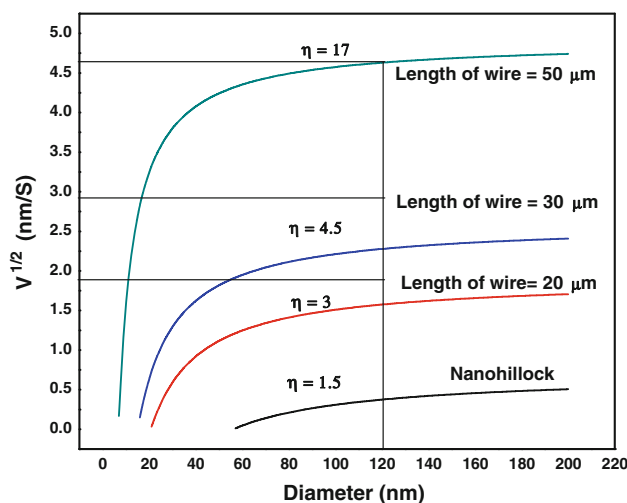


Fig. 1 Theoretical calculation of the growth rate as a function of diameter at 850 °C

phase identification, respectively. Absorption measurements were done with Cary5000 UV–VIS–IR spectrophotometer.

Hydrogen gas sensitivity of the grown nanostructures was determined in a standard way by measuring the isothermal response of the resistance at a working temperature of 230 °C with a flux of hydrogen gas. Two Al contact pads separated by 0.5 mm were sputter coated on glass slides. Nanostructures mixed in acetone using ultrasonic bath were sprayed in the gap of contacts and then heated at 300 °C for 30 min in air. The thermal treatment improved the nanostructure contact with Al contact pads and helped oxygen adsorb on the ZnS nanostructures. The sensors were then placed in a quartz tube for the sensing tests, which was first evacuated, and then 5% H₂ and 95% N₂ gases mixture was introduced through a mass flow controller for sensing measurements.

3 Results and discussions

Figure 2a–d shows the SEM micrographs of ZnS nanostructures synthesized at different substrate temperatures and gas flow rates. Figure 2a–c shows various kinds of nanostructures grown at 850 °C but at different carrier gas flow rates. In the first experiment with the 20 Sccm flow rate, very high density tens of microns long nanowires with average diameter in the range of 120 ± 30 nm were obtained as shown in Fig. 2a. This shows that high supersaturation condition was achieved since the growth rate of nanowires depends on the supersaturation condition, which is controlled by the gas flow rate (which actually affects the flux of the ZnS vapors).

In the second experiment performed at a low flow rate (~ 2 Sccm), zero dimension (0-D) nanostructures were obtained, rather than 1D as shown in Fig. 2b. The average diameters of the 0-D nanostructures were 275 ± 33 nm with the particles average number density was 8×10^8 cm⁻². At this low flow rate, the supersaturation condition was not obtained and the effect of line tension dominated to limit the growth of 1-D nanostructures. As a result 0-D structures were synthesized. With decrease in substrate temperature, the average size of the 0-D structures dropped and density increased, which is due to decrease in the diffusion of particles on the surface. At 675 °C, the average diameters and densities of the 0-D nanostructures were 140 ± 46 nm and 4.4×10^9 cm⁻², respectively. The average diameter of 0-D structures grown at 460 °C was found to be 13 ± 2 nm with average particles number density was 5×10^{10} cm⁻². The large size and low density of 0-D structures at high temperature is evidence of high surface diffusion. XRD patterns revealed

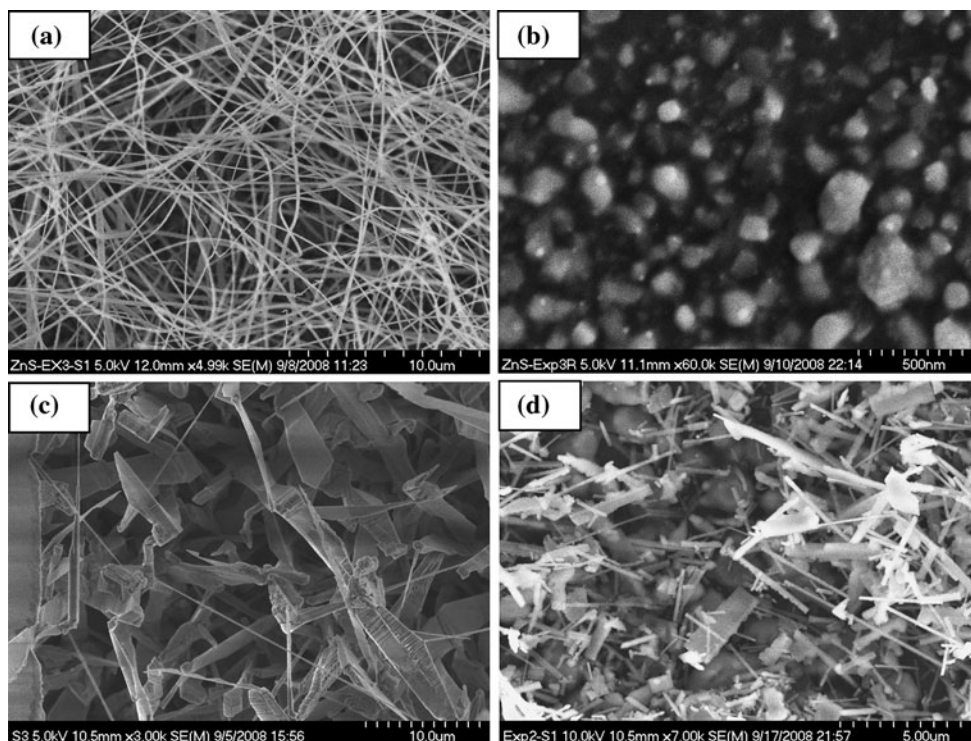
that at low flow rate, a blend of 0-D ZnS and ZnO structures were grown. This is discussed later.

In the third experiment performed at a higher flow rate (~ 60 Sccm), nanostructures were grown with different morphologies at different substrate temperatures. At 850 °C, the high density nanoleaves, many microns long were obtained as shown in Fig. 2c. The average width of nanoleaves was 3.5 ± 0.5 μ m with a thickness of 100 ± 20 nm as determined from SEM images. Nanoleaves were synthesized due to extremely high supersaturation condition and the availability of polar surfaces of ZnS. ZnS in the Wurtzite structure has Zn as a reactive agent and S as an inert agent. Thus at a high supersaturation state when atoms were readily available to the polar surfaces, growth in other directions was also possible but at a slower growth rate.

At low substrate temperature of 675 °C with a flow rate of 20 Sccm, high density of ultra thin nanorods with average diameters of 60 ± 15 nm and length in hundreds of nanometers were grown as shown in Fig. 2d. In addition to this, belts or platelet like 2-D structures were also observed. It is believed that this is due to change in flux of source during heating up and cooling down of the furnace. The platelets like structures were observed only at 675 °C, thus the variation in the supersaturation conditions led to the growth of 2D structures as well. In addition to this, when ZnS is evaporated, Zn and S disassociates and reach catalyst at a different rate, which causes formation of either Zn terminated or S terminated surfaces and the growth is affected due to this. In conclusion, it is worth mentioning that these experimental observations can be explained with the theory with reasonable accuracy as plotted in Fig. 1.

Figure 3a–c shows the X-ray diffraction (XRD) patterns of three distinct nanostructures, nanodots (Fig. 3a), nanowires (Fig. 3b), and nanoleaves (Fig. 3c) synthesized at 850 °C. The XRD pattern from nanodots grown with a low flow rate of 2 Sccm also show presence of low ordered crystalline structures of ZnO as shown and marked in the Fig. 3a. Oxides of Zn are formed as the carrier gas flow rate is too low to obtain sufficient supersaturation condition at the substrate surface for the nanowire growth. This inhibits the growth of crystal at the L-S interface. Oxidation took place due to the presence of oxygen in the native oxide of Si, which could not be flushed out due to very low flow rate. Peaks at around 45 and 69 degrees are due to disordered Si surface. At 850 °C, the desorption of oxygen from the Si surface modified the surface morphology. On the other hand, nanowires and nanoleaves growth is at high supersaturation conditions and this is responsible for the crystallization at the L-S interface. ZnS nanowires grown under these conditions have shown formation of Zinc blend and Wurtzite-2H highly crystalline structures as marked in the Fig. 3b. The percentages of Zinc blend and Wurtzite

Fig. 2 SEM images of growth at 850 °C. **a** Nanowires, grown with 20 Sccm flow rate. **b** Nanodots, grown with 2 Sccm flow rate. **c** Nanoleaves, grown with 60 Sccm flow rate. **d** SEM image of growth of nanorods at 675 °C with 20 Sccm flow rate



phases were 53 and 47%, respectively. The *c/a* value of the Wurtzite 2-H structure obtained was 1.63. The XRD pattern from nanoleaves also demonstrated that ZnS nanostructures are Zinc blend (69%) and Wurtzite-2H (31%) in nature as marked in Fig. 3c. The calculated *c/a* ratio was 1.625, which is lower than observed for nanowires. This is possibly due to the stress produced at high flow rate as XRD peaks are broader in the case of nanoleaves.

The absorption spectroscopy is a simple technique to determine the absorption band edge of semiconductors and to distinguish between different phases in a material, in general. The absorption spectra obtained from the nanodots, nanowires and nanoleaves are shown in the Fig. 4a–c. The absorption spectrum from nanodots (Fig. 4a) shows the presence of mixed phases of the ZnS and ZnO. The peak centered at 3.12 eV is due to ZnO and at 3.60 eV is due to Zinc blend ZnS. From the intensities, it is quite evident that ZnO phase is a minority phase and the width of the peak reflects that it is a disordered phase. The absorption edge for ZnS is not sharp, which shows that ZnS has low order of crystalline structure and existence of defects. This is consistent with the XRD patterns, where peaks emerging from ZnO and ZnS were observed on a background decaying intensity. The absorption spectra of nanowires (Fig. 4b) and nanoleaves (Fig. 4c) show both phases of ZnS crystal, i.e., Zinc blend and Wurtzite. The sharpness of the band edges in both Figures also confirmed that these phases are pure. The determined band gaps from the absorption measurements in the case of Zinc blend ZnS

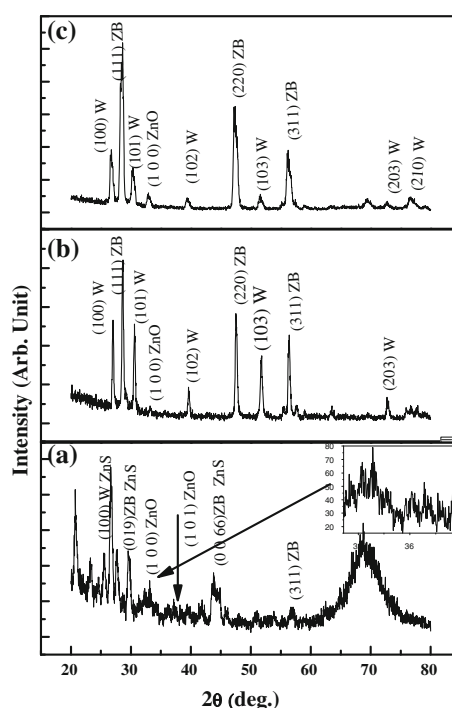
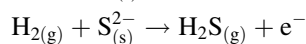
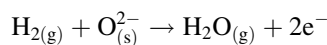


Fig. 3 XRD graphs of **a** nanodots **b** nanowires and **c** nanoleaves

are 3.56 and 3.60 eV for the nanowires and nanoleaves while in the case of Wurtzite ZnS these are 3.89 and 3.91 eV, respectively. No absorption was observed at around 3.12 eV confirming the absence of ZnO phase in these samples. This is consistent with the observation in the

XRD diffraction patterns from nanowires and nanoleaves, where no diffraction was observed from ZnO.

The fundamental sensing mechanism of ZnS based gas sensors is based on a change in the electrical conductivity due to the interaction between gas molecules to be detected and the surface complexes such as O^- , O^{2-} , and/or reactive chemical species (S^{2-}) [1]. After the growth, the ZnS nanostructures were exposed to air and it is anticipated that oxygen adsorbed on the surface of the nanostructures act as negatively charged ions by capturing free electrons from the semiconductor ZnS. This causes the variation in conductance of nanostructures in the presence of H_2 either due to the reaction on the material surface or by removal of chemisorbed oxygen from the surface by H_2 , as shown in the following reaction:



The H_2 gas sensitivity was observed to depend on the morphology of the nanostructure, which increased rapidly from nanodots to nanoleaves to nanorods to nanowires. The sensitivity was calculated by using the relation $S = \frac{R_o - R_{gas}}{R_{gas}}$, here R_o is the resistance before the gas exposure and R_{gas} is the resistance after the gas exposure. Figure 5a–c shows normalized response from (1) nanowires (2) nanodots, and (3) nanoleaves, under identical conditions. It is worth mentioning that response actually depends on adsorption of hydrogen and the conductivity of the structures. Nanowires showed a very quick response towards sensing the

hydrogen as shown in Fig. 5a. For nanowires, $R_o = 1.05 \times 10^8 \Omega$ and $R_{gas} = 1.2 \times 10^7 \Omega$ so the measured sensitivity was 8. Under the same sensing environment, nanodots showed a less sensitive behavior towards the hydrogen gas as shown in Fig. 5b. For nanodots $R_o = 2.16 \times 10^7 \Omega$ and $R_{gas} = 2.07 \times 10^7 \Omega$, so the measured sensitivity was 0.04 while response time was also high about 40 Seconds. Nanoleaves were even found less sensitive towards the hydrogen gas with $R_o = 5.5 \times 10^6 \Omega$ and $R_{gas} = 5.4 \times 10^6 \Omega$, so measured sensitivity was 0.02 with a response time was 50 s, as shown in Fig. 5c.

It is also well known that nanostructures grown by VLS mechanism are single crystal in nature. One of the possible reasons for faster response time is the longer lengths of these nanostructures, allowing better conduction due to small number of contacts/grain boundaries between the wires/particles. The observed response time (time required to reach the 90% of the total response) for the nanowires and nanorods is less than 1 s. Surface cohesive energies play a key role in the sensing characteristics of nanostructures. Nanowires have higher cohesive energy than nanoleaves, thus showing faster response. Although, the exact reason for the higher sensitivity and response time of ZnS nanowires is not obvious, but it is believed to be associated to the adsorption configuration of the gases at the sulphur sites on the surface. Finally, it is deduced from the sensitivity measurements that nanowires sensor is advantageous over nanoleaves sensor for three distinct reasons. First, nanowire structure has large surface-to-volume ratio which means that a significant fraction of the atoms can participate in surface reactions. Second, the Debye length for nanowire is comparable to their radius over a wide temperature and doping range, which makes them more sensitive than nanoleaves. Third, the nanowire is usually stoichiometrically controlled better than nanoleaves, and has a greater order of crystallinity than the nanoleaves.

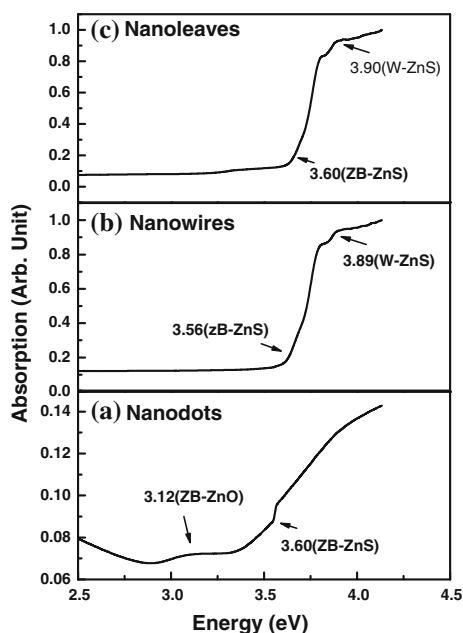


Fig. 4 Absorption spectroscopy graph of **a** nanodots **b** nanowires and **c** nanoleaves

4 Conclusions

ZnS nanostructures of different morphologies and sizes were successfully synthesized by carefully controlling the substrate temperatures and carrier gas flow rates. By controlling these parameters, supersaturation was controlled in different regions of the tube for the growth of different morphologies. It was observed that the experimental findings are in good agreement with the theoretical calculations. Highly crystalline and highly sensitive 1D nanostructures were obtained at the flow rate of 20 Sccm at high temperatures. These showed excellent phase purity with sharp band edge and excellent response to hydrogen gas sensing characteristics with a response time is less than 1 s for the

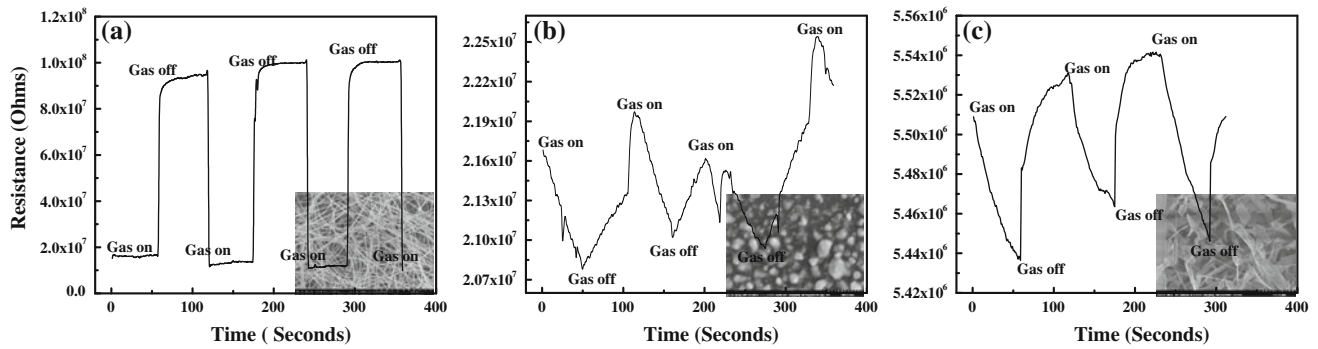


Fig. 5 Isothermal response of **a** nanowires **b** nanodots and **c** nanoleaves, towards 50,000 ppm H_2 gas at the working temperature of 230 °C

1D ZnS nanostructures and response sensitivity of 8, much higher than dots and leaves.

Acknowledgments The work was funded by HEC research grant # 261 and HEC development project “Designing and fabrication of Micro and Nano Devices for applications.” One of the authors, MH is thankful to HEC for PhD scholarship.

References

- Z.G. Chen, J. Zou, G. Liu, H.F. Lu, F. Li, G.Q. Lu, H.M. Cheng, *Nanotechnology* **19**, 055710 (2008)
- O. Lupan, G. Chai, L. Chow, *Micro. Electron. Eng.* **85**, 2220 (2008)
- B. Wang, L.F. Zhu, Y.H. Yang, N.S. Xu, G.W. Yang, *J. Phys. Chem. C* **112**, 6643 (2008)
- C. Shakin, J. Birman, *Phys. Rev.* **109**, 818 (1958)
- D. Moore, Z.L. Wang, *J. Mater. Chem.* **16**, 3898 (2006)
- Y.Y. Wu, P.D. Yang, *J. Am. Chem. Soc.* **123**, 3165 (2001)
- P.D. Rack, P.H. Holloway, *Mater. Sci. Eng. Res.* **21**, 171 (1998)
- T.V. Prevenslik, *J. Lumen* **87**, 1210 (2000)
- P. Calandra, M. Goffredi, V.T. Liveri, *Colloids Surf. A* **160**, 9 (1999)
- S. Kishimoto, A. Kato, A. Naito, Y. Sakamoto, S. Iida, *Phys. Stat. Sol.* **1**, 391 (2002)
- X.Y. Kong, Z.L. Wang, *Nano Lett.* **3**, 1625 (2003)
- X. Fang, Y. Bando, C. Ye, G. Shen, D. Golberg, *J Phys. Chem. C* **111**, 8469 (2007)
- Y.C. Zhu, Y. Bando, D.F. Xue, D. Golberg, *Adv. Mater.* **16**, 9 (2004)
- X. Fang, Y. Bando, M. Liao, U.K. Gautam, C. Zhi, B. Dierre, B. Liu, T. Zhai, T. Sekiguchi, Y. Koide, D. Golberg, *Adv. Mater.* **21**, 1 (2009)
- H.Y. Lu, S.Y. Chu, C.C. Chang, *J. Cry. Gr.* **280**, 173 (2005)
- X.S. Fang, H. Ye, L.D. Zhang, Y.H. Wang, Y.C. Wu, *Adv. Funct. Mater.* **15**, 1 (2005)
- R.S. Wagner, W.C. Ellis, *Appl. Phys. Lett.* **4**, 89 (1964)
- J. Johansson, B. Wacaser, K.A. Dick, W. Seifert, *Nanotechnology* **17**, 355 (2006)
- C. Borchers, D. Stichtenoth, S. Muller, D. Schwen, C. Ronning, *Nanotechnology* **17**, 1071 (2006)
- X. Fang, Y. Bando, C. Ye, G. Shen, D. Golberg, *J. Phys. Chem. C* **111**, 8469 (2007)
- N. Li, T.Y. Tan, U. Gösele, *Appl. Phys. A* **86**, 433 (2007)
- E.I. Givargizove, *J. Cryst. Growth* **31**, 20 (1975)
- S. Li, J.S. Lian, Q. Jiang, *Chem. Phys. Lett.* **455**, 202 (2008)